Fouling mechanisms of ultrafiltration membranes fouled with whey model solutions

María-José Corbatón-Báguena*, Silvia Álvarez-Blanco, María-Cinta Vincent-Vela

Department of Chemical and Nuclear Engineering, Universitat Politècnica de València, C/Camino de Vera s/n 46022 Valencia, Spain

*Corresponding author: macorba@posgrado.upv.es

Tel: +34963877000 (Ext.: 76383)

Fax: +34963877639 (Ext.: 77639)

Abstract

In this work, three ultrafiltration (UF) membranes with different molecular weight cut-offs (MWCOs) and made of different materials were fouled with several whey model solutions that consisted of bovine serum albumin (BSA) (1 % w/w), BSA (1 % w/w) and $CaCl_2$ (0.06 % w/w in calcium) and whey protein concentrate (WPC) with a total protein content of 45 % w/w at three different concentrations (22.2, 33.3 and 44.4 $g \cdot L^{-1}$). The influence of MWCO and membrane material on the fouling mechanism dominating the UF process was investigated. Experiments were performed using two flat-sheet organic membranes and a ceramic monotubular membrane whose MWCOs were 5, 30 and 15 kDa, respectively. Hermia's models adapted to crossflow UF, a combined model based on complete blocking and cake formation equations and a resistance-in-series model were fitted to permeate flux decline curves. The results demonstrated that permeate flux decline was accurately

predicted by all the models studied. However, the models that fitted the best to permeate flux decline experimental data were the combined model and the resistance-in-series model. Therefore, complete blocking and cake formation were the predominant mechanisms for all the membranes and feed solutions tested.

Keywords: Ultrafiltration; whey model solutions; mathematical models; fouling mechanisms.

1. Introduction

Ultrafiltration (UF) membranes have been widely used in dairy industries for several applications such as preconcentration of milk, milk dehydration, fractionation of whey, purification of whey proteins, enrichment of micellar casein for the manufacture of milk, etc. [1, 2].

However, one of the major problems in the UF processes applied in dairy industry is membrane fouling. Among the different substances that are present in milk and whey, proteins are the main responsible for membrane fouling [3]. The most important consequence of fouling is the gradual permeate flux decline during filtration time. This effect depends on different parameters, such as operating conditions of the UF process (crossflow velocity, transmembrane pressure, feed concentration and temperature), interactions between foulants and the membrane surface or membrane characteristics (hydrophilicity, pore size and porosity) [1, 4].

According to the literature, membrane fouling mechanisms can be divided in several types. When the solute molecules are smaller than or similar to the membrane pore size, these molecules can penetrate inside the membrane pores, reducing their effective radius gradually (adsorptive fouling) or causing the entire pore to be completely blocked (pore blocking mechanism) [5, 6]. If solute molecules are much higher than membrane pores, they are deposited on membrane surface. In some cases, the deposited fouling layer may form a cake layer [7, 8].

Because of the technical and economical importance of permeate flux decline, determining the optimum operating conditions to minimize fouling and obtaining a model to predict permeate flux decline with time are key steps in UF processes. Previous studies found in the literature have developed permeate flux decline models for UF processes [9-13]. Among them, empirical models are the most often used due to their high prediction accuracy because they describe experimental results by fitting a mathematical equation to the data obtained without considering any theoretical parameter (examples of these models are those provided by regression analysis) [14]. However, as the theoretical description of fouling phenomena and mechanisms is not reflected on the mathematical equation proposed by this type of models, the relationship between permeate flux decline and the fouling mechanism involved in the UF process cannot be explained with empirical models. On the other hand, theoretical models are able to explain the fouling phenomena during membrane filtration, although they are less accurate. For those reasons, semi-empirical models, which use simplified forms of scientific laws and include a certain number of parameters with physical meaning are more appropriate to provide accurate predictions of the permeate flux decline and also to describe the fouling mechanism at the same time [5, 15, 16].

Although several mathematical models can be found in the literature to explain the fouling mechanisms affecting UF membranes [9, 13, 17, 18], Hermia's models [19] applied to dead-end filtration and their adaptations to crossflow UF are widely used to fit the experimental data of different UF processes. Previous studies found in the literature have demonstrated that Hermia's models can accurately predict permeate flux decline at different experimental conditions. Mohammadi and Esmaeelifar [20] analyzed the fouling mechanisms involved in the UF of wastewaters from a vegetable oil factory working at 3 bar and 0.5 m/s with a 30 kDa polysulfone membrane. Their results demonstrated that fouling was due to the cake layer formation mechanism, achieving a value of R^2 of 0.99. Vincent Vela *et al.* [15] investigated the fouling mechanisms involved in PEG UF using a ceramic membrane of 15 kDa. They obtained that intermediate blocking model was dominant for a transmembrane pressure of 3 bar and a crossflow velocity of 1 m/s and in the case of 4 bar and 2 m/s, with values of R^2 of 0.980 and 0.979, respectively. Salahi *et al.* [5] studied the UF of oily wastewaters using a polyacrylonitrile membrane of 20 kDa at different transmembrane pressures (1.5, 3 and 4.5 bar) and crossflow velocities (0.25, 0.75 and 1.25 m/s). For all the experimental conditions tested, the cake layer formation model followed by the intermediate blocking model were the models that fitted the best, with values of R^2 ranging from 0.9852 to 0.9999 in the case of the cake layer formation model and ranging from 0.8710 to 0.9321 for the intermediate blocking model. Kaya *et al.* [21] applied conventional Hermia's models to predict the fouling mechanism of two nanofiltration membranes (0.4 and 1 kDa) using a paper machine circulation wastewater as feed solution. The best fitting accuracy (R^2 = 0.985) was obtained for the cake layer filtration mechanism followed by the intermediate blocking mechanism (R^2 = 0.982) at a transmembrane pressure of 8 bar.

De la Casa *et al.* [22] combined two fouling mechanisms of Hermia's models. They proposed two different combinations: the first one considers that only a fraction of membrane surface pores (α) is completely blocked (complete blocking model equation) while part of the foulant molecules may pass through the membrane and be adsorbed on the pore walls that were previously unblocked (1-α) (standard blocking model equation). The second combination takes into account that a cake layer of foulant molecules (cake layer formation model equation) can be formed on the previously deposited molecules that have previously completely blocked the pores (complete blocking model equation). The combined models were fitted to the experimental data obtained during the microfiltration of 0.25 $g \cdot L^{-1}$ BSA solutions at a transmembrane pressure of 1 bar and a crossflow velocity of 3.28 $m \cdot s^{-1}$.

On the other hand, the resistance-in-series model is one of the most widely used empirical models due to its high accuracy. Choi *et al.* [23] applied a resistance-in-series model to batch microfiltration of BSA. They considered that total resistance was the sum of the membrane resistance, the cake layer resistance and the fouling resistance. This last one represented the foulant deposits inside the membrane pores. Flux decline predicted by the model was in a good agreement with the experimental data obtained. Carrère *et al.* [24] used a resistance-in-series model to predict permeate flux decline of lactic acid fermentation broths crossflow filtration at a transmembrane pressure of 2 bar and a crossflow velocity of 4 $m \cdot s^{-1}$. Their model considered four different resistances (the membrane resistance, the resistance of the adsorbed molecules on the membrane surface, the resistance due to concentration polarization and the cake layer resistance). They obtained a good agreement between predicted and experimental data.

The aim of this work was to investigate the fouling mechanisms that affect different UF membranes (two polymeric membranes of 5 and 30 kDa and a ceramic monotubular membrane of 15 kDa) using several whey model solutions (BSA (1 % w/w), BSA (1 % w/w) and $CaCl_2$ (0.06 % w/w in calcium) and whey protein concentrate (WPC) with a protein content of 45 % at three different concentrations (22.2, 33.3 and 44.4 $g \cdot L^{-1}$)) as feed solutions during the fouling step. For this purpose, several models were fitted to the experimental data obtained during the UF of whey model solutions: Hermia's models adapted to crossflow UF, a resistance-in-series model and a combined model based on the complete blocking and cake layer formation fouling mechanisms. As a novelty, the last model was developed for this work based on the Hermia's equations adapted to crossflow for the two fouling mechanisms considered. The influence of both membrane MWCO and material on the dominating fouling mechanism was investigated. The values of model parameters were estimated for the models with the highest fitting accuracy. Different equations that relate model parameters with operating conditions such as the membrane roughness and the particle size and the protein concentration of the feed solutions were developed.

2. Modelling

2.1. Hermia's models

The models developed by Hermia [19] are based on classical constant pressure dead-end filtration equations. They consider four main types of membrane fouling: complete blocking, intermediate blocking, standard blocking and cake layer formation. These

models can be adapted to consider a crossflow configuration [15, 25, 26]. Adapted models to crossflow ultrafiltration incorporate the flux associated with the back-transport mass transfer, which is evaluated at the steady-state [27]. The general equation for Hermia's models adapted to crossflow ultrafiltration is shown in Eq. 1:

$$-\frac{dJ}{dt} = K\left(J - J_{ss}\right)J^{2-n} \qquad \text{Eq. 1}$$

where J is the permeate flux, K is a model constant and J_{ss} is the permeate flux when the steady-state is achieved.

According to the value of the parameter n, four different models can be distinguished, based on four different fouling mechanisms: complete blocking (n = 2), intermediate blocking (n = 1), standard blocking (n = 1.5) and cake layer formation (n = 0).

In the complete blocking model, a solute molecule that settles on the membrane surface blocks a pore entrance completely, but it cannot penetrate inside the pores. This model assumes that a monomolecular layer is formed on the membrane surface.

The intermediate blocking model is similar to the complete blocking one because it considers that fouling takes place on the membrane surface and not inside the pores. However, intermediate blocking model allows solute molecules to deposit on previously settled ones.

The standard blocking model takes into account that all the membrane pores have the same length and diameter and the solute molecules are smaller than the membrane pore size. Therefore, these molecules can penetrate inside the pores.

When the solute molecules are larger than the membrane pores, they may accumulate on the membrane surface forming a permeable cake layer. This is the basis of the cake layer formation model.

2.2. Combined model

A combined model based on the crossflow Hermia's equations for complete blocking and cake layer formation was used to predict the permeate flux decline along the whole filtration curve. According to other authors [9, 22, 25], typical variation of permeate flux with time involves two fouling mechanisms: a pore blocking during the first minutes of operation that causes a rapid flux decline and a long term flux decline due to the accumulation of foulant molecules on the membrane surface that results in a cake layer formation.

Therefore, the decline in the permeate flux is the sum of the decline due to the complete blocking model and the decline due to the cake layer formation one. Therefore, two model constants have been taken into account: K_c for the complete blocking model and K_g for the cake layer formation model. The combined model also considers that only a fraction of membrane pores are completely blocked (α). Thus, the general equation of the combined model is Eq. 2:

$$J_{\text{combined model}} = \alpha J_{\text{complete blocking model}} + (1-\alpha) J_{\text{cake layer formation model}} \quad \text{Eq. 2}$$

2.3. Resistance-in-series model

Resistance-in-series model is based on the Darcy's law that relates the permeate flux with the transmembrane pressure and the total hydraulic resistance (Eq. 3):

$$J = \frac{\Delta P}{\mu \cdot R} \quad \text{Eq. 3}$$

where ΔP is the transmembrane pressure, μ is the feed solution viscosity and R is the total hydraulic resistance.

The total hydraulic resistance can be expressed as the sum of different resistances that take place during the UF process. In this model, the membrane resistance, the cake layer resistance and the adsorption and concentration polarization resistances were considered (Eq. 4).

$$J = \frac{\Delta P}{\mu \cdot (R_m + R_a + R_g)} \quad \text{Eq. 4}$$

where R_m is the new membrane resistance, R_a is the resistance due to adsorption on membrane surface and inside its pores and concentration polarization and R_g is the cake layer resistance. In addition, R_a can be fitted using an exponential equation [23, 24]. Therefore, the general equation for the resistance-in-series model is Eq. 5:

$$J = \frac{\Delta P}{\mu \cdot \left(R_m + R'_a \left(1 - exp(-bt)\right) + R_g \right)} \quad \text{Eq. 5}$$

where R'_a is the steady-state adsorption and concentration polarization resistance and b is the fouling rate due to adsorption.

3. Experimental

3.1. Materials

BSA, BSA and $CaCl_2$ and WPC solutions were used as feed solutions to perform the fouling experiments. All these products were supplied in powder form, and were dissolved in deionized water until the desired concentration was achieved for each feed solution. Mean particle size of the feed solutions was determined using a Zetasizer Nano ZS90 (Malvern Instruments Ltd., United Kingdom). BSA (prepared by heat shock fractionation, lyophilized powder, 98 % purity, A3733) was provided by Sigma-Aldrich (Germany), $CaCl_2$ (95 % purity) was purchased from Panreac (Spain) and WPC with a total protein content of 45 % was supplied by Reny Picot (Spain). The composition of the WPC 45 % is shown in Table 1. The following methods were used to estimate the amount of each component in the WPC: bicinchoninic acid method (BCA, Sigma-Aldrich, Germany) for total protein determination [28], 3,5-dinitrosalicylic acid (DNS, Sigma-Aldrich, Germany) reaction to estimate the amount of lactose [29], method of incineration in a muffle furnace at 540 ºC for ash content estimation according to the AOAC method 930.30 [30] and cationic chromatography using a "790 Personal IC" chromatograph equipped with a Metrosep C 2 150 column (both supplied by Metrohm, Switzerland) to determine the

amount of individual cations. Fat content was measured by a MilkoScan FT120 (Gerber Instruments, Switzerland).

BSA and WPC are the most widely used compounds to prepare whey model solutions for UF experiments [1, 31, 32]. In addition, $CaCl_2$ was previously used to study the effect of salts on protein fouling [33-35].

3.2. Membranes

Three UF membranes of different materials and MWCOs were used in the experiments: a monotubular ZrO_2-TiO_2 INSIDE CéRAM^{TM} membrane of 15 kDa (TAMI Industries, France), a flat-sheet polyethersulfone (PES) membrane of 5 kDa (Microdyn Nadir, Germany) and a flat-sheet permanently hydrophilic polyethersulfone (PESH) membrane of 30 kDa (Microdyn Nadir, Germany). The ceramic membrane was 20 cm long with an internal diameter of 0.6 cm and an external diameter of 1 cm and its effective area was 35.5 cm^2. Both polymeric membranes had an effective area of 100 cm^2.

The membranes selected in this work were widely used for treating wastewaters from different industrial fields, such as dye industries [36], pulping plants [37], surface water [38], activated sludge plants [39] and dairy model solutions [40, 41], obtaining in all cases high rejection values.

3.3. Experimental set-up

A VF-S11 UF plant (Orelis, France) was used to perform the fouling experiments in a total recirculation mode. The main parts of the plant are a 10 L feed tank, a temperature regulating system, a variable speed volumetric pump to control the crossflow velocity, two manometers at both sides of the membrane module to measure the transmembrane pressure and a balance (0.001 g accuracy). This experimental set-up is described in [40].

3.4. Experimental procedure

Prior to each fouling experiment, a permeability test with deionized water was performed in order to determine the values of R_m for each membrane used. These values were obtained from the Darcy's law above mentioned (Eq. 3).

Different feed solutions, which contained BSA (1 % w/w), BSA (1 % w/w) and $CaCl_2$ (0.06 % w/w in calcium) and WPC (22.2, 33.3 and 44.4 $g \cdot L^{-1}$), were considered in the fouling tests. Experimental conditions during the fouling step were a transmembrane pressure of 2 bar, a crossflow velocity of 2 $m \cdot s^{-1}$ and a temperature of 25 ºC. The pH values of the feed solutions prepared were in the range 5.97-6.5. The duration of the fouling tests was 2 h. Those conditions were selected according to previous studies on whey ultrafiltration [42] because they are commonly used in whey UF. Those conditions also resulted in severe membrane fouling and thus, clear differences among model predictions can also be achieved. During the experiments, the permeate flux was monitored.

After the fouling step, membranes were rinsed with deionized water during 30 min at a temperature of 25 ºC, a transmembrane pressure of 1 bar and a crossflow velocity of 2.18

$m \cdot s^{-1}$ (for the polymeric membranes) and 4.20 $m \cdot s^{-1}$ (for the ceramic membrane). This difference in the values of crossflow velocity was due to the higher membrane roughness of the ceramic membrane in comparison to the polymeric ones. NaCl solutions at a salt concentration of 5 mM, 50 ºC and the same operating conditions of transmembrane pressure and crossflow velocity as those used in the rinsing step were used to clean the membranes during 60 min. After the cleaning procedure, a last rinsing with deionized water was performed again. Further description of the rinsing/cleaning protocols can be found in [40]. Finally, to recover the initial membrane permeability if the cleaning procedure with NaCl was not completely effective, the ceramic membrane was cleaned with NaClO aqueous solutions (10 % w/v, Panreac, Spain) at 45 ºC and a pH of 11 and the polymeric membranes were cleaned with NaOH aqueous solutions (98 % purity, Panreac, Spain) at 45 ºC and a pH of 11.

Mathematical models were fitted to the experimental data using the MathCad® Genfit algorithm. The Genfit algorithm minimizes the overall difference between experimental results and the predicted ones by means of an optimized version of the Levenberg-Marquadt method. Fitting accuracy of each model was evaluated in terms of the regression coefficient (R^2) and the standard deviation (SD).

3.5. AFM measurements

Membranes roughness was measured by using a Multimode Atomic Force Microscope with a NanoScope V controller (Veeco, Santa Barbara, CA, USA) in a tapping mode of imaging at room conditions and recorded images are shown in Fig. 1. Membrane roughness of samples of 5 μm × 5 μm was measured and the results were presented as the

Root Mean Square roughness (R_q). It takes into account the standard deviation of the surface height values in a certain area, according to Eq. 6 [43]:

$$R_q = \sqrt{\frac{\sum \left(Z_i - Z_{avg}\right)^2}{N_p}} \qquad \text{Eq. 6}$$

Where Z_i is the height value currently measured, Z_{avg} is the average of the height values and N_p is the number of points in the selected area.

4. Results and discussion

The values of the mean particle size of the feed solutions were 3.497±0.078, 4.386±0.705 and 132.000±8.283 nm for the BSA, BSA and $CaCl_2$ and WPC solutions, respectively. The values of the R_m for the membranes used in the experiments were $9.453 \cdot 10^{12}$, $5.001 \cdot 10^{12}$ and $3.794 \cdot 10^{12}$ m^{-1} for the membranes of 5, 15 and 30 kDa, respectively.

Figs. 2 to 6 show the experimental permeate flux decline observed for all the membranes tested during the UF of different feed streams. In Figs. 2-6 permeate flux predictions by means of the three models that showed the highest accuracy (highest R^2 and lowest SD, see Tables 2-6) are represented for each membrane and feed solution considered. Comparing the permeate flux obtained at different WPC concentrations for the same membrane, it can be observed that it decreased as WPC concentration increased for all the membranes tested because the fouling became more severe when WPC concentration increased. In addition, for all the feed solutions tested, the PESH 30 kDa membrane showed the lowest permeate flux decline in comparison with the PES 5 kDa membrane and the ceramic 15 kDa

membrane. For example, permeate flux decline was 21.45, 45.60 and 50.97 % for the 30, 5 and 15 kDa membranes, respectively, for the most severe fouling conditions (WPC 45 % at 44.4 $g \cdot L^{-1}$). The reason for that is the hydrophilic nature of the 30 kDa membrane. According to other authors [44, 45], the best antifouling properties (high rejection coefficient, low permeate flux decline and low total filtration resistance) corresponds to the most hydrophilic membranes. Rahimpour and Madaeni [44] tested several PES membranes during the crossflow filtration of non-skim milk. Their results demonstrated that the hydrophilic PES membranes had a lower permeate flux decline (about 16 %) than the unmodified hydrophobic PES membrane (about 40 %).

In addition, membrane fouling is also related to the surface roughness. Evans *et al.* [46] demonstrated that rougher surfaces favour the entrapment of foulant molecules. This phenomenon can be observed for all the membranes tested comparing permeate flux decline with the Root Mean Square roughness values (R_q) for each membrane tested. The highest flux decline was achieved for the 15 kDa membrane (R_q = 17.900 nm), followed by the 5 kDa membrane (R_q = 0.487 nm and hydrophobic) and the 30 kDa membrane (R_q = 1.657 nm and hydrophilic) [41]. This pattern was in accordance with the results obtained by García-Ivars *et al.* [45]. They demonstrated that PES 30 kDa membranes with high hydrophilicity and low surface roughness had the lowest permeate flux decline during several fouling/rinsing cycles compared with other modified and unmodified PES membranes with higher surface roughness and hidrophobicity.

Tables 2 to 6 show the fitting accuracy for the Hermia's models adapted to crossflow, the combined model and the resistance-in-series model for all the membranes and feed solutions tested. All the models fitted with almost the same accuracy to the experimental

data, with the only exception of the standard blocking model. The fitting accuracy of the standard blocking model (n = 1.5) was very low for all the experimental data considered in this work. Therefore, this model was not considered. This can be explained by the fact that solute molecules were larger than the membrane pores, as in the case of the BSA and BSA and $CaCl_2$ feed solutions [4]. In the case of WPC 45 % feed solutions, at the pH values of the solutions prepared in this work (5.97), the lowest molecular weight proteins tend to form dimers that are larger than the pore size of the membranes [47, 48]. Therefore, they cannot penetrate inside the porous structure. In Tables 2-6, the models with the best fitting accuracy are highlighted in bold for each membrane and feed solution tested. As it can be observed in Table 2, the combined model was the best for all the membranes when BSA was used as feed solution. When BSA and $CaCl_2$ solutions were ultrafiltered (see Table 3), the combined model had the highest fitting accuracy for the polymeric membranes (5 and 30 kDa). However, the resistance-in-series model had a slightly higher value of R^2 for the 15 kDa ceramic membrane fouled with BSA and $CaCl_2$. In the case of WPC 45 % solutions (Tables 4-6), the model that fitted the best to the experimental data was the resistance-in-series model for all the membranes, except for the 5 kDa membrane when WPC 45 % at the highest concentration (44.4 $g \cdot L^{-1}$) was tested. In this last case, the best model was the combined one. However, in some cases it is difficult to select the best fitting model between the combined and the resistance-in-series one, such as in the case of the 15 kDa membrane using BSA (Table 2). According to other authors [9, 22], the decrease in permeate flux with time can be divided in two stages: first, a rapid flux decline due to a pore blocking phenomena and, after that, a slow decrease until the steady-state is achieved due to the formation of a cake layer. These two stages are those that are considered in the combined model. The resistance-in-series model takes into account both fouling mechanisms as well as it considers the resistance due to adsorption of solute molecules on

the membrane surface and inside its pores and the resistance caused by the cake layer. Therefore, according to both models, both mechanisms (pore blocking and cake layer formation) must be considered to explain membrane fouling when whey model solutions (BSA, BSA and $CaCl_2$ and WPC solutions) are ultrafiltered.

The values of model parameters for the best fitting models are shown in Table 7. When BSA was used as feed solution, the values of the pore blocking parameter, α, indicate that cake layer formation was the predominant fouling mechanism for all the membranes tested. This result is also in agreement with the individual analysis of Hermia's models adapted to crossflow in the case of BSA solutions (see Table 2). The reason can be that solute molecules (67 kDa) are much larger than the pores of the 5, 15 and 30 kDa membranes, thus solute molecules are accumulated on the membrane surface, forming a layer on it. Regarding the values of the cake layer formation model parameter, K_g, and the complete blocking model parameter, K_c, for the 5, 15 and 30 kDa membranes and BSA solutions (Table 7), both parameters decreased when the MWCO increased. It is important to note that one of the hypotheses of the Hermia's complete blocking model is that the pore entrance is completely blocked or sealed when one solute molecule arrives at the membrane surface. Therefore, both models (complete blocking and cake layer formation) consider membrane fouling mechanisms that are external and occur on the membrane surface [49]. According to Brião and Tavares [49], these external membrane fouling mechanisms are related to the difference between the solute molecule size and the membrane pore size. This difference is higher as the MWCO decreases. Thus, a greater amount of particles can be deposited on the membrane surface and a tighter bound cake layer may be formed on the membrane with the lowest MWCO (5 kDa). On the other hand, according to the membrane material, hydrophilic membranes usually have better

antifouling properties than those made of hydrophobic materials [44-46]. As the 30 kDa membrane was a PESH membrane, the fouling was less severe using the same feed solution and experimental conditions as in the case of the 5 kDa PES membrane. In addition, as it was above mentioned, the lower the membrane roughness is, the less severe the membrane fouling is. For the membranes tested in this work, the roughness of the PESH 30 kDa membrane is very low and similar to that of the hydrophobic PES 5 kDa membrane. However, the surface roughness of the ceramic 15 kDa membrane is much greater. Therefore, the combination of high hydrophilicity and low surface roughness favour the low permeate flux decline observed for the 30 kDa membrane.

When BSA and $CaCl_2$ solutions were used as feed solutions, the best fitting accuracy was obtained with the combined model for the polymeric membranes (5 and 30 kDa). In this case, comparing the values of the parameters when BSA solutions were used and those calculated for BSA and $CaCl_2$ solutions, it can be observed that the values of both parameters considered in this model (K_c and K_g) increased to a large extent when BSA and $CaCl_2$ were fed simultaneously. Therefore, fouling was more severe when $CaCl_2$ was added to the feed solutions. Calcium salts have been demonstrated to act as bridging agents between proteins, agglomerating them [33, 34]. Almécija *et al.* [33] investigated the effect of calcium salts on the UF of whey solutions. They reported that the percentage of membrane blocked pores during UF increased as the concentration of calcium salts increased in the feed solution. Ang and Elimelech [34] studied the fouling of reverse osmosis membranes using BSA and calcium solutions. They demonstrated that, when calcium concentration increased, permeate flux decline was greater because the electrostatic repulsion among BSA molecules is diminished. De la Casa *et al.* demonstrated that Hermia's models parameters increased as the membrane fouling was more severe

during the microfiltration of BSA [22]. According to their work, permeate flux reduction and thus, membrane fouling, was greater at values of pH near the isoelectric point of the protein, when protein agglomeration occurs as well. Comparing the values of the Hermia's cake layer formation parameter, they observed that these values increased as membrane fouling was more severe (at pH 7). On the other hand, comparing the values of the model parameters K_c and K_g for the 5 and 30 kDa when BSA and $CaCl_2$ solutions were fed, it can be observed that both parameters decreased as membrane MWCO increased. It indicates a lower permeate flux decline and thus, less severe membrane fouling in the case of the 30 kDa membrane. This pattern is in agreement with that obtained for BSA solutions.

The resistance-in-series model was the model with the highest fitting accuracy when WPC 45 % solutions at a concentration of 22.2 and 33.3 $g \cdot L^{-1}$ were used as feed for all the membranes tested and also for the 15 and 30 kDa membranes using WPC 45 % solutions at 44.4 $g \cdot L^{-1}$. Comparing the values for the model parameters R'_a and R_g, it can be observed that they increased as the MWCO decreased for all the membranes tested. The increase in model parameters with the membrane MWCO is in agreement with the results previously commented for the other feed solutions. In addition, for the 15 and 30 kDa membranes, the values of R'_a and R_g increased when WPC concentration increased from 22.2 to 44.4 $g \cdot L^{-1}$, indicating greater membrane fouling as feed concentration increased. For the 5 kDa membrane, R_g also increased when WPC concentration increased from 22.2 to 33.3 $g \cdot L^{-1}$. However, the value of R'_a was similar for both WPC concentrations. This can be due to the fact that, because of the great difference between the proteins size and the membrane pore size, the possibility of adsorption inside the pores is lower in the case of the membrane with the lowest MWCO (5 kDa) in comparison with the other membranes. Thus, the value of R'_a is similar independently of the WPC concentration.

In order to generalize the values of the model parameters for different membranes, feed solutions and protein concentrations in the feed solution; the model parameters for the two best fitting models (resistance-in-series and combined models) were correlated to three independent variables (membrane surface roughness, mean particle size of the feed solution and protein concentration in the feed solutions) using a multiple regression analysis from Statgraphics®. The developed equations that relate the values of model parameters (Table 7) to the three independent variables and their combinations at a confidence interval of 95 % (p-values lower than 0.05) are Eqs. 7-12. The accuracy of these equations (Eqs. 7-12) in terms of R^2 was 0.973, 0.926, 0.988, 0.974, 0.984 and 0.971, respectively.

$$R'_a = 1.330 \cdot 10^{13} - 9.212 \cdot 10^{12} \cdot R_q + 4.394 \cdot 10^{10} \cdot r + 4.589 \cdot 10^{11} \cdot {R_q}^2 + 9.359 \cdot 10^{10} \cdot R_q \cdot C_b \qquad \text{Eq. 7}$$

$$b = 8.207 \cdot 10^{-4} - 2.891 \cdot 10^{-4} \cdot R_q + 1.506 \cdot 10^{-5} \cdot {R_q}^2 - 4.405 \cdot 10^{-7} \cdot {C_b}^2 \qquad \text{Eq. 8}$$

$$R_g = 2.660 \cdot 10^{13} - 1.399 \cdot 10^{13} \cdot R_q + 4.611 \cdot 10^{10} \cdot r + 7.263 \cdot 10^{11} \cdot {R_q}^2 + 2.020 \cdot 10^{10} \cdot {C_b}^2 \qquad \text{Eq. 9}$$

$$K_c = 192.336 - 162.484 \cdot R_q + 0.130 \cdot r + 5.210 \cdot {R_q}^2 - 0.302 \cdot {C_b}^2 + 6.215 \cdot R_q \cdot C_b \qquad \text{Eq. 10}$$

$$K_g = -1.998 \cdot 10^9 + 4.528 \cdot 10^7 \cdot R_q + 2.773 \cdot 10^8 \cdot C_b - 2.363 \cdot 10^4 \cdot r^2 - 7.712 \cdot 10^6 \cdot {C_b}^2 - 4.604 \cdot 10^6 \cdot R_q \cdot C_b + \\ + 1.825 \cdot 10^5 \cdot R_q \cdot r \qquad \text{Eq. 11}$$

$$a = 7.490 \cdot 10^{-1} - 4.783 \cdot 10^{-2} \cdot C_b - 2.425 \cdot 10^{-3} \cdot {R_q}^2 - 3.608 \cdot 10^{-5} \cdot r^2 - 4.504 \cdot 10^{-3} \cdot R_q \cdot C_b - 2.089 \cdot 10^{-4} \cdot R_q \cdot r$$

Eq. 12

These equations can be used to predict the best conditions resulting in the lowest possible fouling and thus, in the highest steady-state permeate flux. In the case of the resistance-in-series model, which was one of the most accurate for the experimental data obtained for all the membranes and feed solutions tested, the general model equation (Eq. 5) indicated that the highest steady-state permeate flux was obtained when R'_a and R_g had a value of 0. Therefore, an optimization analysis was performed by means of the Microsoft Excel Solver tool in order to determine the values of the independent variables in Eqs. 7-9 that made R'_a and R_g equal to 0. These values were a membrane surface roughness of 1.605 nm, a particle size of 1.374 nm and a protein concentration in the feed solution of 1.647 $g \cdot L^{-1}$. As it was above mentioned, the lower the protein concentration in the feed solution and its particle size are, the less aggregates are formed and thus, the lower the membrane fouling is. In addition, rougher surfaces allow solute molecules to deposit on them, favouring membrane fouling [45, 46].

5. Conclusions

The models studied in this work can predict with high accuracy the experimental permeate flux for all the membranes tested when different whey model solutions that contained BSA (1 % w/w), BSA (1 % w/w) and $CaCl_2$ (0.06 % w/w in calcium) and WPC with a total protein concentration of 45 % w/w (22.2, 33.3 and 44.4 $g \cdot L^{-1}$) were ultrafiltered at 2 bar and 2 m/s. By fitting experimental data to all these models, the predominant fouling mechanisms were confirmed for all the membranes and feed solutions tested. Only the Hermia's standard blocking model did not show a very accurate fitting to the experimental

data, because solute molecules were much higher than membrane pore size, thus they cannot penetrate inside the membrane porous structure.

According to the accuracy of models fitting, the resistance-in-series model and the combined model achieved the highest R^2 and lowest SD for all the feed solutions and membranes tested. This indicates that both cake layer formation and pore blocking contributed to membrane fouling.

The combination of high hydrophilicity and low surface roughness resulted in a membrane with better antifouling behaviour. Thus, the 30 kDa membrane showed the lowest permeate flux decline and the lowest values of model parameters for all the feed solutions tested.

Acknowledgements

The authors of this work wish to gratefully acknowledge the financial support of the Spanish Ministry of Science and Innovation through the project CTM2010-20186.

Nomenclature

List of symbols

b	Fouling rate due to adsorption (s^{-1})
C_b	Protein concentration in the feed solution ($g \cdot L^{-1}$)
K	Hermia's model constant (units depending on n)
K_c	Complete blocking model constant (s^{-1})

K_g	Cake layer formation model constant ($s \cdot m^{-2}$)
J	Permeate flux ($m^3 \cdot m^{-2} \cdot s^{-1}$)
J_{model}	Permeate flux predicted by each model ($m^3 \cdot m^{-2} \cdot s^{-1}$)
J_{ss}	Steady-state permeate flux ($m^3 \cdot m^{-2} \cdot s^{-1}$)
n	Hermia's model parameter (dimensionless)
N_p	Number of points within the selected area (dimensionless)
ΔP	Transmembrane pressure (bar)
r	Mean particle size (nm)
R	Total hydraulic resistance (m^{-1})
R_a	Resistance due to adsorption on membrane surface and inside its pores and concentration polarization (m^{-1})
R'_a	Steady-state adsorption resistance
R_g	Cake layer resistance (m^{-1})
R_m	New membrane resistance (m^{-1})
R_q	Root Mean Square Roughness (nm)
t	Filtration time (s)
Z_{avg}	Average of the height values of the sample (nm)
Z_i	Value of height currently measured (nm)

Greek letters

α	Fraction of membrane pores completely blocked (dimensionless)
μ	Feed solution viscosity ($kg \cdot m^{-1} \cdot s^{-1}$)

Abbreviations

BSA	Bovine serum albumin
MWCO	Molecular weight cut off
PES	Polyethersulfone
PESH	Permanently hydrophilic polyethersulfone
UF	Ultrafiltration
WPC	Whey protein concentrate

References

[1] M.O. Nigam, B. Bansal, X.D. Chen, Fouling and cleaning of whey protein concentrate fouled ultrafiltration membranes, Desalination 218 (2008) 313-322.

[2] M. Kazemimoghadam, T. Mohammadi, Chemical cleaning of ultrafiltration membranes in the milk industry, Desalination 204 (2007) 213-218.

[3] M.A. Argüello, S. Álvarez, F.A. Riera, R. Álvarez, Enzymatic cleaning of inorganic ultrafiltration membranes used for whey protein fractionation, J. Membr. Sci. 216 (2003) 121-134.

[4] C. Wang, Q. Li, H. Tang, D. Yan, W. Zhou, J. Xing, Y. Wan, Membrane fouling mechanism in ultrafiltration of succinic acid fermentation broth, Biores. Technol. 116 (2012) 366-371.

[5] A. Salahi, M. Abbasi, T. Mohammadi, Permeate flux decline during UF of oily wastewater: experimental and mmodeling, Desalination, 251 (2010) 153-160.

[6] R.A. Ruby Figueroa, A. Cassano, E. Drioli, Ultrafiltration of orange press liquor: Optimization for permeate flux and fouling index by response surface methodology, Sep. Purif. Technol. 80 (2011) 1-10.

[7] C. Tien, B.V. Ramarao, On analysis of cake formation and growth in cake filtration, J. Chin. Inst. Chem. Eng. 37 (2006) 81-94.

[8] J. Kim, F.A. DiGiano, Fouling models for low-pressure membrane systems, Sep. Purif. Technol. 68 (2009) 293-304.

[9] C-C. Ho, L. Zydney, A combined pore blockage and cake filtration model for protein fouling during microfiltration, J. Colloid Interface Sci. 232 (2000) 389-399.

[10] P.K. Bhattacharya, S. Agarwal, S. De, U.V.S. Rama Gopal, Ultrafiltration of sugar cane juice for recovery of sugar: analysis of flux and retention, Sep. Purif. Technol. 21 (2001) 247-259.

[11] C. Duclos-Orsello, W. Li, C-C. Ho, A three mechanism model to describe fouling of microfiltration membranes, J. Membr. Sci. 280 (2006) 856-866.

[12] R. Peterson, J. Geeting, R. Daniel, Estimation of ultrafilter performance based on characterization data, Chem. Eng. Technol. 30 (2007) 1050-1054.

[13] K.W.K. Yee, D.E. Wiley, J. Bao, A unified model of the time dependence flux decline for the ultrafiltration of whey, J. Membr. Sci. 332 (2009) 69-80.

[14] J. Baranyi, T. Ross, T.A. McMeekin, T.A. Roberts, Effects of parameterization on the performance of empirical models used in “predictive microbiology”, Food Microbiol. 13 (1996) 83-91.

[15] M.C. Vincent Vela, S. Álvarez Blanco, J. Lora García, E. Bergatiños Rodríguez, Analysis of membrane pore blocking models adapted to crossflow ultrafiltration in the ultrafiltration of PEG, Chem. Eng. J. 149 (2009) 232-241.

[16] S-K. Mah, C-K. Chuah, W.P. Cathie Lee, S-P. Cahi, Ultrafiltration of palm oil-oleic acid-glycerin solutions: Fouling mechanism identification, fouling mechanism analysis and membrane characterizations, Sep. Purif. Technol. 98 (2012) 419-431.

[17] C. Bhattacharjee, S. Datta, Analysis of polarized layer resistance during ultrafiltration of PEG-6000: an approach based on filtration theory, Sep. Purif. Technol. 33 (2003) 115-126.

[18] H. Peng, A.Y. Tremblay, Membrane regeneration and filtration modeling in treating oily wastewaters, J. Membr. Sci. 324 (2008) 59-66.

[19] J. Hermia, Constant pressure blocking filtration laws – application to powerlaw non-newtonian fluids, Trans IChemE 60 (1982) 183-187.

[20] T. Mohammadi, A. Esmaeelifar, Wastewater treatment of a vegetable oil factory by a hybrid ultrafiltration-activated carbon process, J. Membr. Sci. 254 (2005) 129-137.

[21] Y. Kaya, Z.B. Gonder, I. Vergili, H. Barlas, The effect of transmembrane pressure and pH on treatment of paper machine process waters by using a two-step nanofiltration process, Desalination 250 (2010) 150-157.

[22] E.J. de la Casa, A. Guadix, R. Ibáñez, F. Camacho, E.M. Guadix, A combined fouling model to describe the influence of the electrostatic environment on the cross-flow microfiltration of BSA, J. Membr. Sci. 318 (2008) 247-254.

[23] S-W. Choi, J-Y. Yoon, S. Haam, J-K. Jung, J-H. Kim, W-S. Kim, Modeling of the permeate flux during microfiltration of BSA-adsorbed microspheres in a stirred cell, J. Colloid Interface Sci. 228 (2000) 270-278.

[24] H. Carrère, F. Blaszkow, H. Roux de Balmann, Modelling the clarification of lactic acid fermentation broths by cross-flow microfiltration, J. Membr. Sci. 186 (2001) 219-230.

[25] R.W. Field, D. Wu, J.A. Howell, B.B. Gupta, Critical flux concept for microfiltration fouling, J. Membr. Sci. 100 (1995) 259–272.

[26] S.T.D. de Barros, C.M.G. Andrade, E.S. Mendes, L. Peres, Study of fouling mechanism in pineapple juice clarification by ultrafiltration, J. Membr. Sci. 215 (2003) 213-224.

[27] C. Jarusutthirak, S. Mattaraj, R. Jiraratananon, Influence of inorganic scalants and natural organic matter on nanofiltration membrane fouling, J. Membr. Sci. 287 (2007) 138-145.

[28] P.K. Smith, R.I. Krohn, G.T. Hermanson, A.K. Mallia, F.H. Gartner, M.D. Provenzano, E.K. Fujimoto, N.M. Goeke, B.J. Olson, D.C. Klenk, Measurement of protein using bicinchoninic acid, Anal. Biochem. 150 (1985) 76-85.

[29] G.L. Miller, Use of dinitrosalicylic acid reagent for determination of reducing sugar, Anal. Chem. 31 (1959) 426-428.

[30] AOAC Official Method 930.30, 1930, Ash of Dried Milk, first action 1930.

[31] Y-N. Wang, C.Y. Tang, Protein fouling of nanofiltration, reverse osmosis, and ultrafiltration membranes-The role of hydrodynamic conditions, solution chemistry and membrane properties, J. Membr. Sci. 376 (2011) 275-282.

[32] A. Afonso, J.M. Miranda, J.B.L.M. Campos, Numerical study of BSA ultrafiltration in the limiting flux regime – Effect of variable physical properties, Desalination 249 (2009) 1139-1150.

[33] M.C. Almécija, A. Martínez-Férez, A. Guadix, M.P. Páez, E.M. Guadix, Influence of the cleaning temperature on the permeability of ceramic membranes, Desalination 245 (2009) 708-713.

[34] W.S. Ang, M. Elimelech, Protein (BSA) fouling of reverse osmosis membranes: Implications for wastewater reclamation, J. Membr. Sci. 296 (2007) 83-92.

[35] H. Mo, K.G. Tay, H.Y. Ng, Fouling of reverse osmosis membrane by protein (BSA): Effects of pH, calcium, magnesium, ionic strength and temperature, J. Membr. Sci. 315 (2008) 28-35.

[36] J. Kawiecka-Skowron, K. Majewska-Nowak, Effect of dye content in a treated solution on performance of the UF ceramic membrane, Environ. Prot. Eng. 37 (2011) 5-12.

[37] Y. Zhang, C-Y. Cao, Q-X. Hou, W-Y. Feng, M. Xu, Z-H. Su, Q-Y. Lin, J-F. Zhuang, W-J. Lv, Using a membrane filtration process to concentrate the effluent from alkaline peroxide mechanical pulping plants, Biores. 5 (2010) 780-795.

[38] M. Kabsch-Korbutowicz, A. Urbanowska, Water treatment in integrated process using ceramic membranes, Polish J. Environ. Stud. 19 (2010) 731-737.

[39] A. Karagündüz, N. Dizge, Investigation of membrane biofouling in cross-flow ultrafiltration of biological suspension, J. Membr. Sci. Technol. 3 (2013) 1-5.

[40] M.J. Corbatón-Báguena, S. Álvarez-Blanco, M.C. Vincent-Vela, Cleaning of ultrafiltration membranes fouled with BSA by means of saline solutions, Sep. Purif. Technol. 125 (2014) 1-10.

[41] M.J. Corbatón-Báguena, S. Álvarez-Blanco, M.C. Vincent-Vela, Salt cleaning of ultrafiltration membranes fouled by whey model solutions, Sep. Purif. Technol. 132 (2014) 226-233.

[42] P. Matzinos, R. Álvarez, Effect of ionic strength on rinsing and alkaline cleaning of ultrafiltration inorganic membranes fouled with whey proteins, J. Membr. Sci. 208 (2002) 23-30.

[43] T.-S. Chung, J.-J. Qin, A. Huan, K.-C. Toh, Visualization of the effect of die shear rate on the outer surface morphology of ultrafiltration membranes by AFM, J. Membr. Sci. 196 (2002) 251-266.

[44] A. Rahimpour, S.S. Madaeni, Improvement of performance and surface properties of nano-porous polyethersulfone (PES) membrane using hydrophilic monomers as additives in the casting solution, J. Membr. Sci. 360 (2010) 371-379.

[45] J. Garcia-Ivars, M-I. Alcaina-Miranda, M-I. Iborra-Clar, J-A. Mendoza-Roca, L. Pastor-Alcañiz, Enhancement in hydrophilicity of different polymer phase-inversion

ultrafiltration membranes by introducing PEG/Al_2O_3 nanoparticles, Sep. Purif. Technol. 128 (2014) 45-57.

[46] P.J. Evans, M.R. Bird, A. Pihlajamäki, M. Nyström, The influence of hydrophobicity, roughness and charge upon ultrafiltration membranes for black tea liquor clarification, J. Membr. Sci. 313 (2008) 250-262.

[47] P.F. Fox, P.L.H. McSweeney (eds), Advanced Dairy Chemistry: Vol. 1: Proteins, third edition, Kluwer Academic/Plenum Publishers, New York, 2003.

[48] O.E. Mills, L.K.A. Creamer, Conformational change in bovine β-lactoglobulin at low pH, Biochem. Biophys. Acta 379 (1975) 618-626.

[49] V.B. Brião, C.R.G. Tavares, Pore blocking mechanism for the recovery of milk solids from dairy wastewater by ultrafiltration, Brazilian J. Chem. Eng. 29 (2012) 393-407.

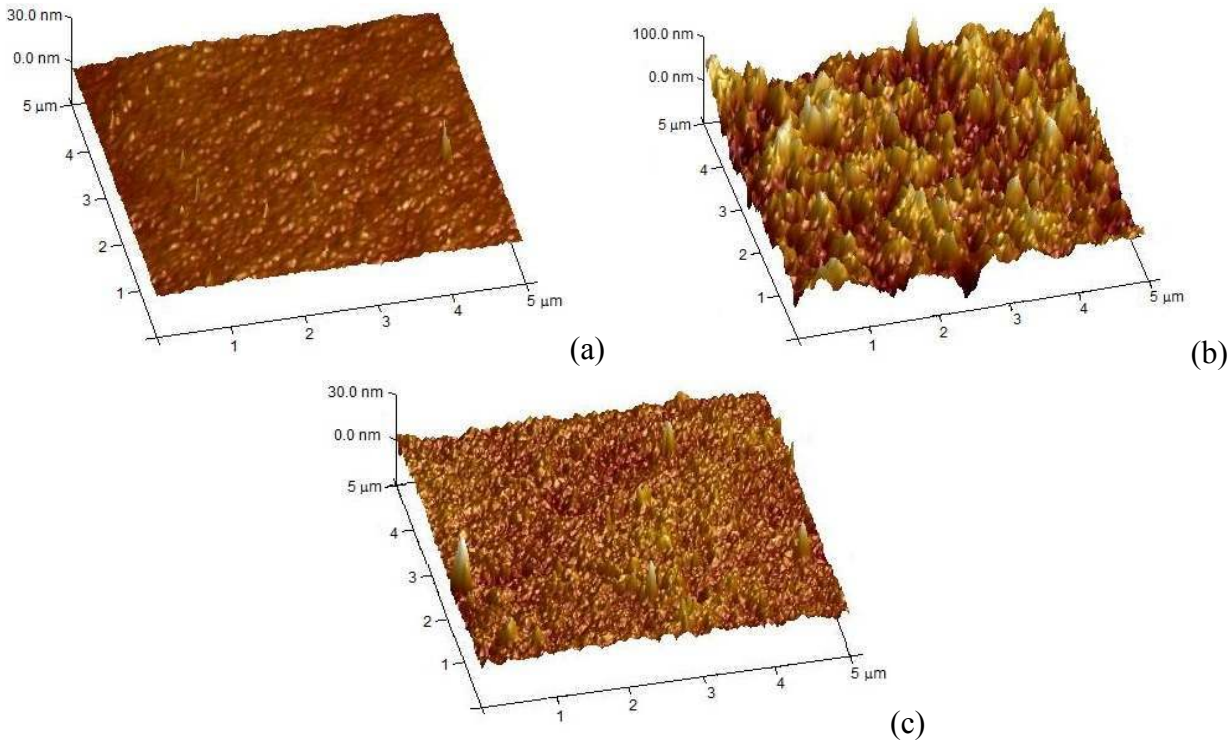

Fig. 1. AFM images for the membranes of (a) 5 kDa, (b) 15 kDa and (c) 30 kDa.

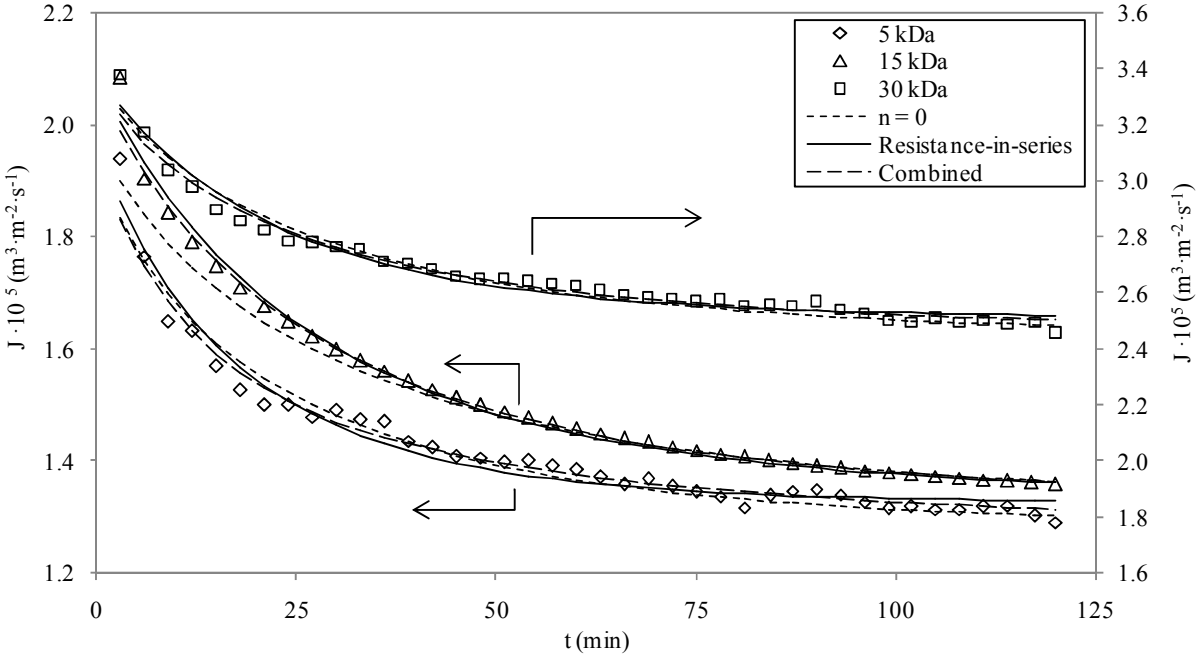

Fig. 2. Permeate flux predictions for the best fitting models during the ultrafiltration of BSA solutions at 2 bar, 2 m·s^{-1} and 25 ºC (lines: estimated results; symbols: experimental data). The highest fitting accuracy corresponded to the combined model (R^2 of 0.972, 0.993 and 0.976 for the 5, 15 and 30 kDa membranes, respectively).

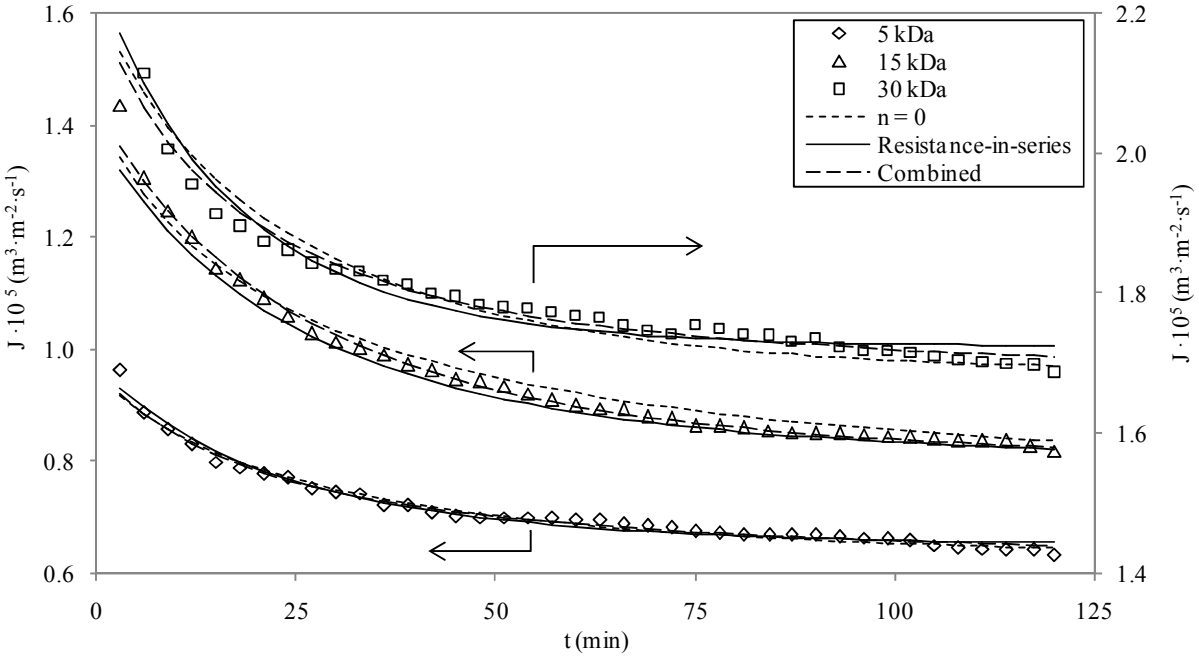

Fig. 3. Permeate flux predictions for the best fitting models during the ultrafiltration of BSA and $CaCl_2$ solutions at 2 bar, 2 $m \cdot s^{-1}$ and 25 ºC (lines: estimated results; symbols: experimental data). The highest fitting accuracy corresponded to the combined model (R^2 of 0.983 and 0.968 for the 5 and 30 kDa membranes, respectively) and to the resistance-in-series model (R^2 of 0.993 for the 15 kDa membrane).

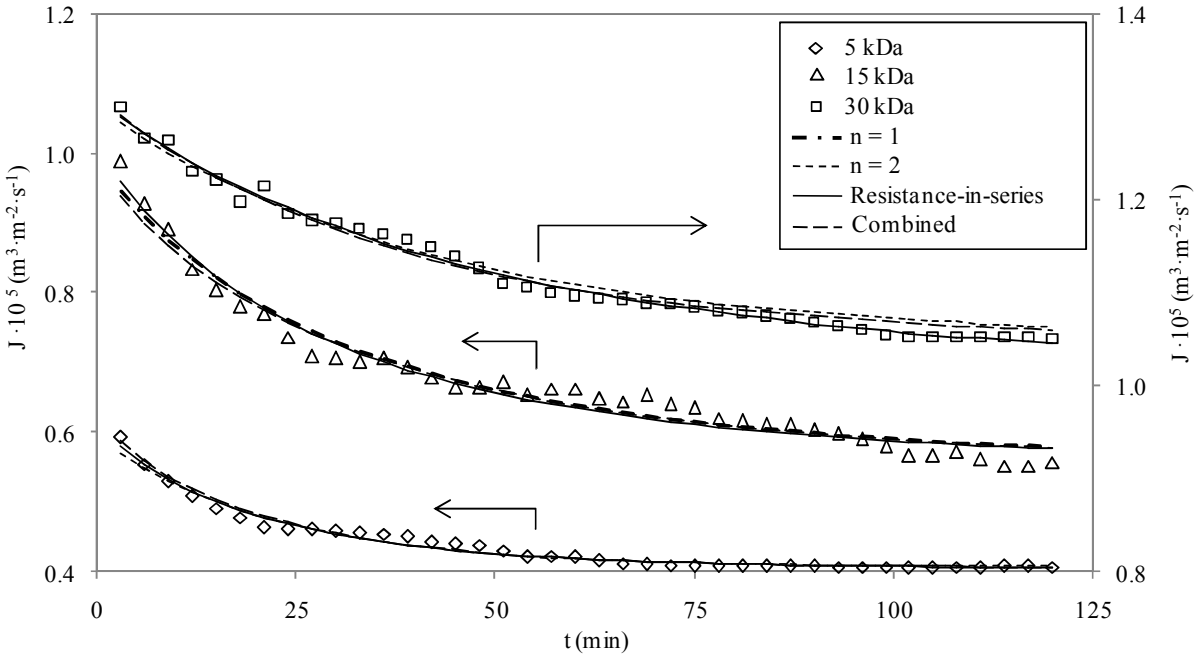

Fig. 4. Permeate flux predictions for the best fitting models during the ultrafiltration of WPC 45 % (22.2 $g \cdot L^{-1}$) solutions at 2 bar, 2 $m \cdot s^{-1}$ and 25 ºC (lines: estimated results; symbols: experimental data). The highest fitting accuracy corresponded to the resistance-in-series model (R^2 of 0.982, 0.969 and 0.991 for the 5, 15 and 30 kDa membranes, respectively).

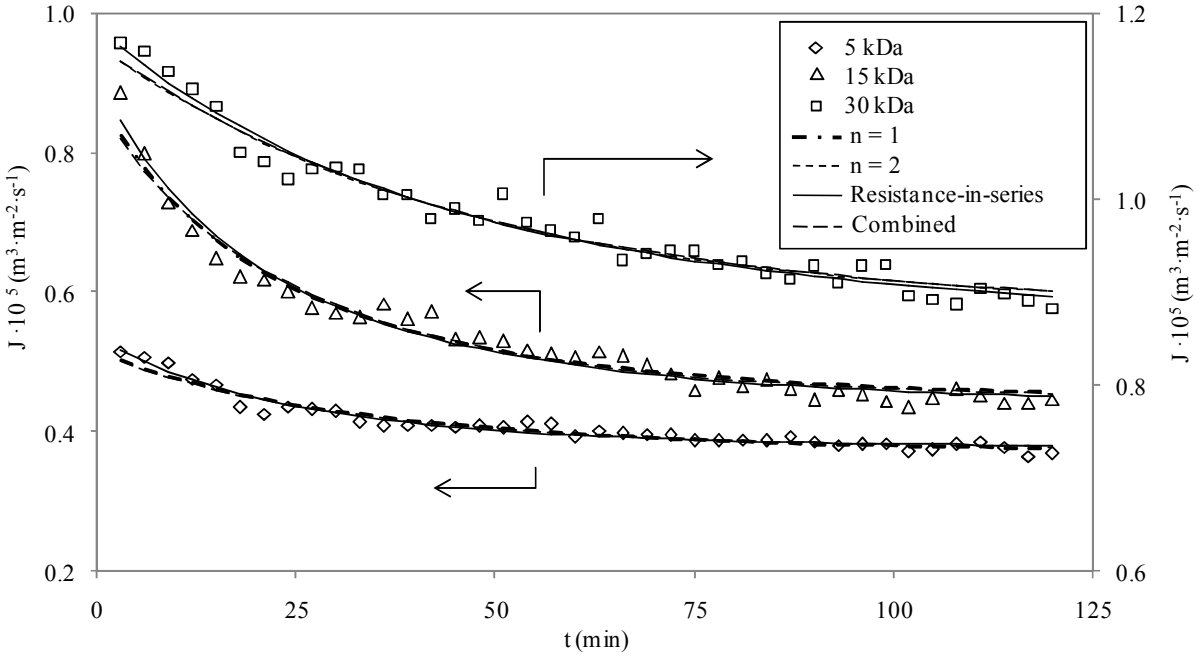

Fig. 5. Permeate flux predictions for the best fitting models during the ultrafiltration of WPC 45 % (33.3 $g \cdot L^{-1}$) solutions at 2 bar, 2 $m \cdot s^{-1}$ and 25 ºC (lines: estimated results; symbols: experimental data). The highest fitting accuracy corresponded to the resistance-in-series model (R^2 of 0.952, 0.971 and 0.968 for the 5, 15 and 30 kDa membranes, respectively).

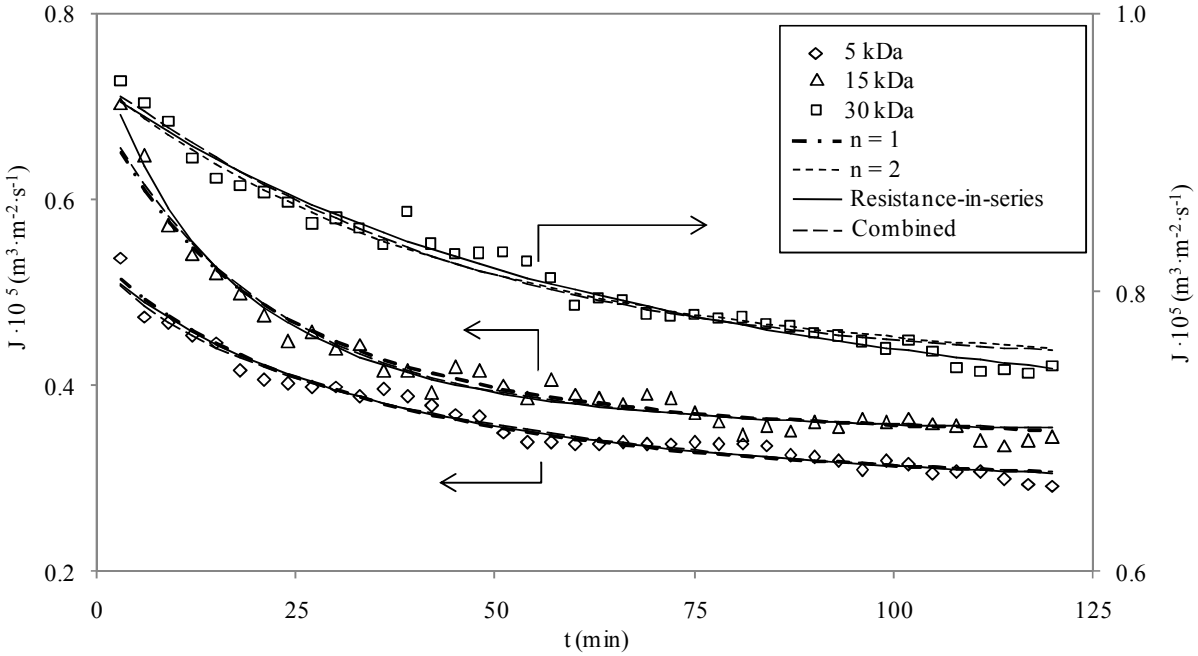

Fig. 6. Permeate flux predictions for the best fitting models during the ultrafiltration of WPC 45 % (44.4 $g \cdot L^{-1}$) solutions at 2 bar, 2 $m \cdot s^{-1}$ and 25 ºC (lines: estimated results; symbols: experimental data). The highest fitting accuracy corresponded to the combined model (R^2 of 0.971 for the 5 kDa membrane) and to the resistance-in-series model (R^2 of 0.979 and 0.980 for the 15 and 30 kDa membranes, respectively).

Table 1.
Composition of WPC 45 % powder.

Component	Value
Total proteins (%)	38.16 ± 0.51
Lactose (%)	42.33 ± 0.16
Fat (%)	9.00 ± 0.45
Ash (%)	6.15 ± 0.07
Ca (%)	0.87 ± 0.08
Na (%)	1.34 ± 0.13
K (%)	1.57 ± 0.01

Table 2.
Models fitting accuracy for the ultrafiltration of BSA solutions at 25 ºC, 2 bar and 2 $m \cdot s^{-1}$: values of R^2 and SD.

MWCO (kDa)	Model	R^2	SD
5	Complete blocking (n = 2)	0.922	0.025
	Intermediate blocking (n = 1)	0.948	0.020
	Cake formation (n = 0)	0.962	0.016
	Combined model	**0.972**	**0.013**
	Resistance-in-series model	0.964	0.017
15	Complete blocking (n = 2)	0.981	0.014
	Intermediate blocking (n = 1)	0.904	0.033
	Cake formation (n = 0)	0.991	0.008
	Combined model	**0.993**	**0.007**
	Resistance-in-series model	0.992	0.008
30	Complete blocking (n = 2)	0.936	0.018
	Intermediate blocking (n = 1)	0.957	0.015
	Cake formation (n = 0)	0.970	0.012
	Combined model	**0.976**	**0.010**
	Resistance-in-series model	0.971	0.012

Table 3.
Models fitting accuracy for the ultrafiltration of BSA and $CaCl_2$ solutions at 25 ºC, 2 bar and 2 $m \cdot s^{-1}$: values of R^2 and SD.

MWCO (kDa)	Model	R^2	SD
5	Complete blocking (n = 2)	0.950	0.022
	Intermediate blocking (n = 1)	0.971	0.016
	Cake formation (n = 0)	0.980	0.013
	Combined model	**0.983**	**0.012**
	Resistance-in-series model	0.980	0.013
15	Complete blocking (n = 2)	0.975	0.024
	Intermediate blocking (n = 1)	0.969	0.026
	Cake formation (n = 0)	0.977	0.022
	Combined model	0.991	0.012
	Resistance-in-series model	**0.993**	**0.012**
30	Complete blocking (n = 2)	0.922	0.017
	Intermediate blocking (n = 1)	0.941	0.015
	Cake formation (n = 0)	0.953	0.013
	Combined model	**0.968**	**0.010**
	Resistance-in-series model	0.965	0.011

Table 4.
Models fitting accuracy for the ultrafiltration of WPC 45 % solutions (22.2 $g \cdot L^{-1}$) at 25 ºC, 2 bar and 2 $m \cdot s^{-1}$: values of R^2 and SD.

MWCO (kDa)	Model	R^2	SD
5	Complete blocking (n = 2)	0.976	0.014
	Intermediate blocking (n = 1)	0.975	0.014
	Cake formation (n = 0)	0.966	0.017
	Combined model	0.980	0.014
	Resistance-in-series model	**0.982**	**0.013**
15	Complete blocking (n = 2)	0.954	0.032
	Intermediate blocking (n = 1)	0.967	0.028
	Cake formation (n = 0)	0.958	0.031
	Combined model	0.966	0.028
	Resistance-in-series model	**0.969**	**0.028**
30	Complete blocking (n = 2)	0.973	0.010
	Intermediate blocking (n = 1)	0.965	0.012
	Cake formation (n = 0)	0.962	0.012
	Combined model	0.982	0.008
	Resistance-in-series model	**0.991**	**0.006**

Table 5.
Models fitting accuracy for the ultrafiltration of WPC 45 % solutions (33.3 $g \cdot L^{-1}$) at 25 ºC, 2 bar and 2 $m \cdot s^{-1}$: values of R^2 and SD.

MWCO (kDa)	Model	R^2	SD
5	Complete blocking (n = 2)	0.936	0.022
	Intermediate blocking (n = 1)	0.941	0.021
	Cake formation (n = 0)	0.938	0.021
	Combined model	0.943	0.032
	Resistance-in-series model	**0.952**	**0.020**
15	Complete blocking (n = 2)	0.957	0.036
	Intermediate blocking (n = 1)	0.967	0.032
	Cake formation (n = 0)	0.949	0.039
	Combined model	0.965	0.032
	Resistance-in-series model	**0.971**	**0.031**
30	Complete blocking (n = 2)	0.962	0.015
	Intermediate blocking (n = 1)	0.958	0.016
	Cake formation (n = 0)	0.948	0.017
	Combined model	0.962	0.015
	Resistance-in-series model	**0.968**	**0.014**

Table 6.
Models fitting accuracy for the ultrafiltration of WPC 45 % solutions (44.4 $g \cdot L^{-1}$) at 25 ºC, 2 bar and 2 $m \cdot s^{-1}$: values of R^2 and SD.

MWCO (kDa)	Model	R^2	SD
5	Complete blocking (n = 2)	0.952	0.032
	Intermediate blocking (n = 1)	0.969	0.027
	Cake formation (n = 0)	0.964	0.029
	Combined model	**0.971**	**0.025**
	Resistance-in-series model	0.969	0.026
15	Complete blocking (n = 2)	0.962	0.036
	Intermediate blocking (n = 1)	0.969	0.031
	Cake formation (n = 0)	0.943	0.040
	Combined model	0.969	0.032
	Resistance-in-series model	**0.979**	**0.030**
30	Complete blocking (n = 2)	0.965	0.013
	Intermediate blocking (n = 1)	0.959	0.014
	Cake formation (n = 0)	0.950	0.016
	Combined model	0.968	0.012
	Resistance-in-series model	**0.980**	**0.009**

Table 7.
Values of model parameters for the best fitting models.

MWCO (kDa)	Feed solution	Resistance-in-series model			Combined model		
		$R'_a \cdot 10^{-13}$ (m^{-1})	$b \cdot 10^{4}$ (s^{-1})	$R_g \cdot 10^{-13}$ (m^{-1})	K_c (s^{-1})	$K_g \cdot 10^{-6}$ ($s \cdot m^{-2}$)	α (dimensionless)
5	BSA	-	-	-	83.519	2.050	0.349
	BSA + $CaCl_2$	-	-	-	112.731	7.287	0.312
	WPC 45 % (22.2 $g \cdot L^{-1}$)	1.877	6.392	2.792	-	-	-
	WPC 45 % (33.3 $g \cdot L^{-1}$)	1.759	5.306	3.212	-	-	-
	WPC 45 % (44.4 $g \cdot L^{-1}$)	-	-	-	65.898	40.590	0.442
15	BSA	-	-	-	30.042	2.012	0.288
	BSA + $CaCl_2$	1.253	4.250	1.015	-	-	-
	WPC 45 % (22.2 $g \cdot L^{-1}$)	1.789	3.664	1.713	-	-	-
	WPC 45 % (33.3 $g \cdot L^{-1}$)	2.633	4.278	1.945	-	-	-
	WPC 45 % (44.4 $g \cdot L^{-1}$)	3.474	5.394	2.409	-	-	-
30	BSA	-	-	-	7.757	1.212	0.312
	BSA + $CaCl_2$	-	-	-	11.913	3.119	0.287
	WPC 45 % (22.2 $g \cdot L^{-1}$)	0.487	2.951	1.330	-	-	-
	WPC 45 % (33.3 $g \cdot L^{-1}$)	0.696	2.941	1.506	-	-	-
	WPC 45 % (44.4 $g \cdot L^{-1}$)	0.836	2.020	1.978	-	-	-